Desalination and Water Treatment
www.deswater.com
doi: 10.5004/dwt.2020.25681

193 (2020) 95–105
July

Preparation and characterization of manganese silicomolybdate for the adsorptive removal of Pb(II) and Fe(III) metal ions from aqueous medium: case study: Hesinia area, Egypt

Yousra H. Kotp*, Mohamed E.A. Ali, Muhammad Gomaah, Hesham A. Ezzeldin

Hydrogeochemistry Department, Desert Research Center, El Matareya Cairo, Egypt 11753, Tel. +20 1 063953608; Fax: +20 2 26389069; email: yoso20002000@yahoo.com (Y.H. Kotp)

Received 6 December 2019; Accepted 12 February 2020

ABSTRACT

Manganese silicomolybdate (Mn–Si–Mo) was prepared using sol–gel technique and employed for Pb^{2+}, and Fe^{3+} adsorption. Scanning electron microscopy, X-ray diffraction, Fourier-transform infrared spectroscopy, dynamic light scattering, thermo-gravimetric analysis/differential thermal analysis, and UV were applied to characterize the prepared exchanger. Experiments using batch were proceeded via the distribution coefficient, isotherms, and thermodynamic. The maximum adsorption capacity was established 8.5 and 6.5 meq/g at 25°C for Pb^{2+}, and Fe^{3+} ions, respectively. Freundlich isotherm successfully fitted for the adsorption of lead and iron ions which implied that the adsorption process was physi sorption, the thermodynamic parameters like $\Delta H°$, $\Delta S°$, and $\Delta G°$ were computed, demonstrating that the adsorption behavior was spontaneous and endothermic in nature. A mechanism describing the interaction of Mn–Si–Mo and different pollutants is briefly explained. The presented low cost-effective material is advanced to prepare Mn–Si–Mo adsorbent for the abstraction of toxic pollutants from real water.

Keywords: Manganese silicomolybdate; Equilibrium studies; Isotherm; Adsorption; Ion exchange

1. Introduction

The Hesinia area is east of the Nile River north Cairo, at latitudes 30°45′ and 31°00′ N and longitudes 31°50′ and 32°5′E. The study area is surrounded at the west by the Nile River (Damietta Branch), Suez Canal at the east, Mediterranean Sea, and Manzala Lake at the north and Ismailia canal at the south (Fig. 1). The eastern Nile Delta is an achieve region for agriculture in Egypt. Some problems come into sight with decreasing Nile water, inequitable convention of groundwater, and irrigation with drainage water. A lot of researchers dedicated their hard work toward learning the sources and origin of these problems and consequences. Review of the beforehand work concerning the water pollution of groundwater in the study area [1]. Fast industrialization has conducted to the enlarged action of serious metals into the surroundings. The enormous growing in serious metals over the precedent little decades has surely gave rise to in an increased streams of metallic materials in the aqueous framework which has an unfavorable effect on the surroundings. Around twenty significant metals are divided as toxic, and 1/2 these released into the atmosphere in quantities that are dangerous to human health [2]. The permissible level for lead and iron in drinking water is 0.05, and 0.3 mg/L, respectively. The permissible limit (mg/L) for Pb(II) and Fe(III) in wastewater, given by the Environmental Protection Agency (EPA), is 0.05 and 0.3 mg/L [3]. In the Hesinia area, the concentration of lead and iron in the groundwater varied from 0 to 3.49 mg/L for iron and from 0 to 0.38 for lead [1].

* Corresponding author.

El Matareya Cairo, Egypt 11753
yoso20002000@yahoo.com

Presented at the 4th International Water Desalination Conference: Future of Water Desalination in Egypt and the Middle East, 24–27 February 2020, Cairo, Egypt

Heavy metal elimination can be accomplished by using traditional treatment methods, for example, chemical precipitation [4,5], ion exchange [6–9], solvent extraction [4,10], and electrochemical deletion [5,10]. These procedures have an important drawback, which is, for example, partial elimination, elevated-energy necessities, and creation of toxic sludge [11]. Newly, many approximations have been considered for the expansion of inexpensive and extra useful technologies, together to reduce the wastewater formed and to develop the excellence of the handled effluent. Adsorption has grown to be a single of the unusual treatments, in current years, the explore for small-cost adsorbents that have metal-required capacities has massives [5,12].

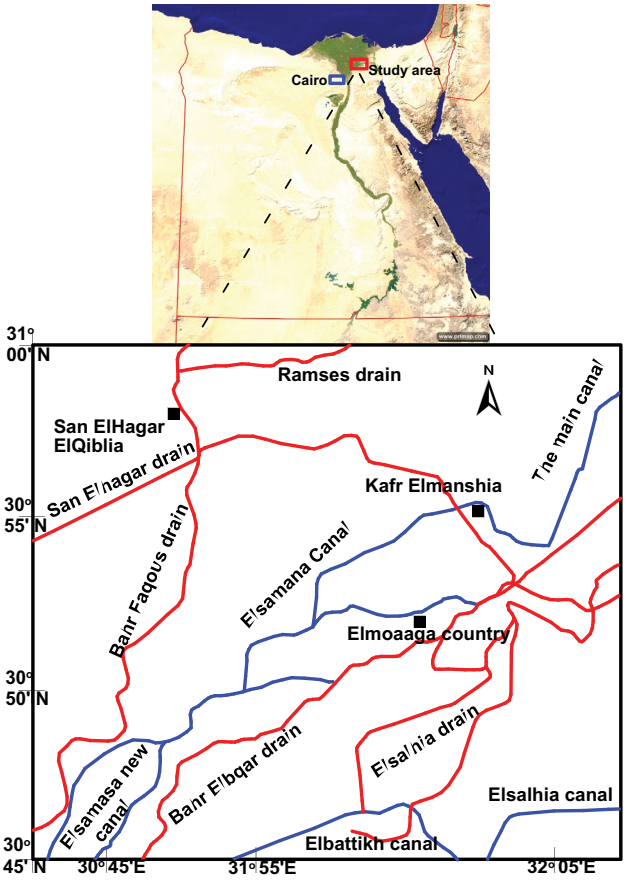

Fig. 1. Location map of the study area (modified after Abo El-Fadl [1]).

Scientific information is currently given a great compact of information involving different adsorbents having a selectively of eliminating serious metal ions from hydrous mixtures. Scientists have revealed rising attention over current times in adsorbents of normal source. Normal sorbents are resources that arise in the surroundings, and whose employ does not transport concerning some additional contamination. The class of choosy adsorbents of normal source contains such materials like sedimentary rocks, peat, coffee grounds, lignin, olive gravels, and several minerals [13–19]. The performance of the adsorption of an individual set of heavy metals from aquatic medium is exaggerated not merely by the kind of sorption material applied, however by procedure setting such as reach time of reagents, absorption of the forerunner of heavy metal ions, pH, temperature, and quantity of adsorbent [20–22]. Values of adsorption capacity Q_0 (mg/g) of the other adsorbents are given in Table 1. In the literature, there is no data regarding sol–gel derived manganese silicomolybdate (Mn–Si–Mo) adsorbent. Therefore, in this study, a challenge was made to use the sol–gel technique for the synthesis of new, active oxide adsorbent used to the elimination of hazardous metal ions like lead and Iron from their solutions. The synthesized adsorbent was investigated in detail, mainly in conditions of its morphology structure. This synthesized adsorbent was obtained via conventional schemes of water or emulsion precipitation, mechanism of sol–gel way permitted to synthesize material described with high purity, short bulk density and definitely better parameters of the porous arrangement, as well as developed surface area. Many sorption tests were completed, including capacity, evaluation of pH, and temperature as well as sorption isotherm.

Table 1
Comparison of adsorption capacity of other adsorbents for Pb(II) and Fe(III)

Metal	Adsorbent	Adsorption capacity (mg/g) of M ion	References
Pb(II)	MnO_2-MOF	917	[23]
	MOF-5	659	[24]
	MIL-53 (Al@100aBDC)	492	[25]
	HS-mSi@MOF-5	312	[26]
	TMU-5	251	[27]
	UiO-66-NHC(S)NHMe	232	[28]
	HKUST-1-MW@$H_3PW_{12}O_{40}$	98	[27]
	Cu-terephthalate MOF	80	[29]
Fe(III)	3D Co(II) MOF or (1)	100	[30]
	Cu-terephthalate MOF	115	[29]

2. Experimental

2.1. Chemical reagents and instruments

The main chemicals worn for the synthesis in this research were manganese chloride tetra hydrate ($MnCl_2{\cdot}4H_2O$) (molecular weight = 197.9, purity ≥ 98%), sodium metasilicate (Na_2SiO_3) (molecular weight = 122.06, purity ≥ 98%), and ammonium molybdate $(NH_4)_6Mo_7O_{24}{\cdot}4H_2O$, M.W = 196.02 g/mole, purity 99.98%), and lead chloride ($PbCl_2$; M.W = 278.11 g/mole, purity ≥ 98%) and ferric chloride ($FeCl_3{\cdot}6H_2O$; M.W = 270.29 g/mole, purity ≥ 99.9%) (Sigma Aldrich, Germany). All reagents presented were of analytical grade. Fourier-transform infrared (FTIR) spectrophotometer (MB 147, Canada). The scanning electron microscopy (SEM) were done using (SEM Quanta FEG), Powder X-ray diffraction (XRD) patterns were made by (Shimadzu X-ray diffractometer, Model XD 490 Shimadzu, Japan). Thermal stabilities, were conceded using (a DT-60H thermal analyzer, Shimadzu, Japan). UV-Vis spectrophotometer (Elico EI 301E, India) and dynamic light scattering (DLS, Malvern Zetasizer Nano-ZS Nano Series).

2.2. Preparation of manganese silicomolybdate

Manganese silicoomolybdate (Mn–Si–Mo) was synthesized by adding (0.3 M) solutions of $MnCl_2{\cdot}4H_2O$ and ammonium molybdate (0.1 M), then Sodium metasilicate (0.3 M) was added drop cleverly until the color of the prepared solution twisted to brown at pH 10.5, and then the suspension solution was reserved in a vacuum incubator at 40°C for 1 d. The suspension was vacuum filtered, and cleaned several times with DI water. The resulting Mn–Si–Mo was dried in an oven at 60°C for 24 h and finally air-dried to appear in dark brown particles.

2.3. Chemical stability

In order to calculate the stability of the prepared material against several media, the chemical stability of Mn–Si–Mo in different acids media (HCl and HNO_3), base (NaOH) was calculated using batch experiments. A quantity of 100 mg portions of Mn–Si–Mo were approached for 24 h at room temperature with 100 mL of a specific medium with intermittently shaking. After contact, the ion exchanger was estranged, then dried at 60°C and the weight losses (%) were considered which appears good chemical stability, improved ion-exchange capacity, and mechanical properties, showing good numerous behavior. This feature is important from a practical point of view, in order to establish the region of adsorbent applicability. The result suggests that the cation-exchange properties of synthetic carbons activated with phosphoric acid are chemically stable in very acid and very basic solution [27,30].

2.4. Adsorption capacity

The ion exchange capacity (meq./g) of Mn–Si–Mo was firmed using a batch technique where,0.5 g of Mn–Si–Mo preheated at different temperature (50°C, 200°C, 400°C, 600°C, and 800°C) was equilibrated with 50 mL of 0.05 mol/dm^3 solution of 0.05 M solutions of Pb^{2+} and Fe^{3+} ions. After equilibration at room temperature, the solution of metal ions was separated and changed by the same volume of the initial solution concentration.

The capacity was computed as the following:

$$\text{capacity} = \frac{\%\text{uptake}}{100} \times C_0 \times \frac{V}{m} \times Z \text{ meq/g} \quad (1)$$

where C_0 is the concentration of the starting solution of lead and iron ions, V are the volume, m is the Mg–Si–Mo mass and Z is the charge of the replaced ions.

2.5. Distribution studies

Dilution of slandered solutions of lead and iron (1,000 mg/L) with deionized water gave required initial solutions with suitable concentration. Proper amounts of Mn–Si–Mo (0.1 g) and 10 mL of desired concentration of Pb and Fe solutions were put into 100 mL Erlenmeyer flask. A constant agitation rate of 180 rpm at different temperature ranging from 25°C to 60°C was forced in an automatic shaker. The pH of lead and Fe solutions was attuned to the different values by putting HNO_3 (1 M) solution. Samples were centrifuged at 3,500 rpm to separate the aqueous solution from the adsorbed material. Later the supernatants were measured using ICPseq-7500 spectrometer and the removal efficiency were computed using the following relation:

$$K_d = \frac{I - F}{F} \times \frac{V}{m} \text{mL/g} \quad (2)$$

where V/m is the relation of solution volume to an adsorbent mass, I and F is the initial and final concentration of metal ions, respectively.

2.6. Sorption isotherms

To evaluate the highest adsorption capacity of adsorbents, isotherms were measured using Pb(II) and Fe(III) concentration ranging between 0 and 500 mg/L,, and adsorption were finalized after 24 h contact time at different temperature of 25°C, 40°C, and 60°C. Pb(II) and Fe(III) concentration in supernatants was deliberated using inductively coupled plasma–atomic emission spectroscopy (ICP–AES). The solution pH for the adsorption isotherm study was 4.9 and 2.9 (±0.05) for lead and iron, respectively. The Freundlich isotherm is a semi-empirical equation that supposes no identical division of heat of adsorption on the varied surface. Freundlich isotherm is given as:

$$q_e = K_f C_e^{1/n} \quad (3)$$

where q_e is the equilibrium sorption capacity (mg/g), K_f and n are the Freundlich parameters and C_e is the symmetry concentration (mg/L).

2.7. Column experiment

Experimental arrangement worn for the dynamic column studies was done for adsorptive removal of lead and iron from contaminated wastewater from Hesinia area, Egypt,

using granulated Mn–Si–Mo. This experiment consists of column of silicate glass of 20 mm diameter. Supernatant after passing though the columns were discharged into a sump below the column. Previously wetted and degassed Mn–Si–Mo is packed up to give bed height (m) in water filled column of 20 mm (internal diameter). Column is placed vertically and Mn–Si–Mo bed is supported on plate. The operation is in down run plug style. The sorption tests were accomplished at room temperature 25°C ± 2°C and initial pH of 5.0. The residual concentration of both metal ions in aqueous media was calculated by using ICP–AES as before. The break-through capacities (mg/g) of the lead and iron ions were considered and computed from the Eq. (4):

$$\text{Break-through capacity} = V_{(50\%)} \times \frac{C_0}{m}\left(\text{meq}/\text{g}\right) \quad (4)$$

where $V_{50\%}$ is the volume at to break-through in cm^3, Z is the valance of the ion, C_0 is the preliminary concentration of lead and iron element in mg/mL, and m is the weight of the Mn–Si–Mo bed (g).

3. Results and discussion

3.1. Characterization of Mn–Si–Mo cation exchanger

To assess the involvement of the prepared Mn–Si–Mo exchanger on different oxides, FTIR spectra of Mn–Si–Mo (Fig. 2) were analyzed and showed several bands in 790–1,100 cm^{-1} regions which could likely be accredited to the symmetric silicon oxide and silicon hydroxide and asymmetric Si–O–Si vibrations [31–33]. which, in addition to the peaks mentioned, showed abroad peak at ~3,450 cm^{-1} and an intense peak centered at ~1,610 and 1,040 cm^{-1}, assigned to the water O–H groups bending to Mn–Si–Mo exchanger and these peaks could not be totally eliminated by heating the exchanger at 200°C, 400°C, 600°C, and 800°C, but its intensity however, decreased [34,35]. Finally, the peaks at 500–900 cm^{-1}, characteristic of Mo–O stretching vibrations [36,37], could prove the presence of molybdate as impurities. The surface morphology of the Mn–Si–Mo particles obtained after drying at 50°C for 24 h is shown in Fig. 3. By using SEM micrographs demonstrate that amorphous particles were obtained. These primary particles showed a big tendency to aggregate and form larger particle clusters.

Fig. 4 shows an X-ray powder diffraction pattern of precipitated Mn–Si–Mo dried at different drying temperature. The spectrum appears as different crystalline bands with the equivalent Bragg angle at 2θ = 12.5°, 17°,23.5°, 24°, 26.5°, 28°, 29°, 31°, 31°, 33°, 34°, 37°, and 41°, which pointed to the material is crystalline. The smoothness of the band also specified that numerous washings with deionized water were capable in eliminating the NaCl impurities attentive in the pores of the gel network. The occurrence of quick peaks proves the presence of crystallinity arrangement in Mn–Si–Mo materials. However, the prepared Mn–Si–Mo exchanger has dissimilar crystalline phases with lower size at special drying temperatures, these leading to numerous site exchanges, high selectivity, and capacity for different ions [36]. It can be obvious from Table 2, that all Mn–Si–Mo dried at different drying temperature show a high degree of crystallinity with slight changes. These changes may be attributed to the presence of different drying conditions. Fig. 5 shows thermo-gravimetric analysis (TGA) and differential thermal analysis (DTA) curve of Mn–Si–Mo exchanger. Two endothermic occurrence peaks take place up to 255°C, owing to the evaporation of adsorbed water [38–40]. From 0°C to 490°C, TGA diagram show two stages of weight losses with a total weight loss equal to 3.9%. The third weight loss occurs at 900.8°C with a total weight loss 11.55% this weight loss can be resulted from the processes of hydrolysis and condensation of silicate molecules [41,42]. Fig. 6 shows the electronic absorption spectra of Mn–Si–Mo and examined by UV-Vis spectrophotometer in the range of 500–710 nm and the medium is taken in the UV

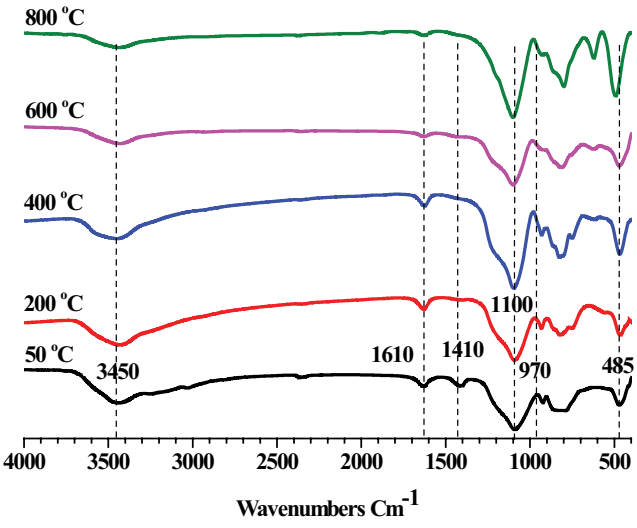

Fig. 2. FT-IR spectrum of Mn–Si–Mo at different drying temperatures.

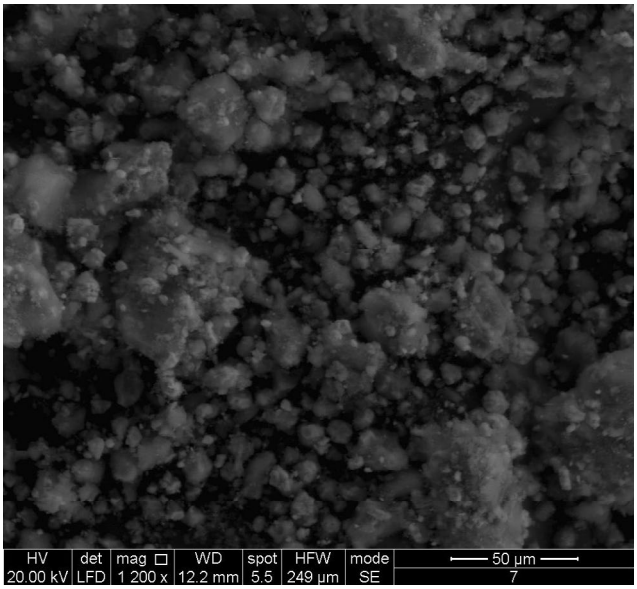

Fig. 3. Scanning electron microscope image of Mn–Si–Mo dried at 50°C.

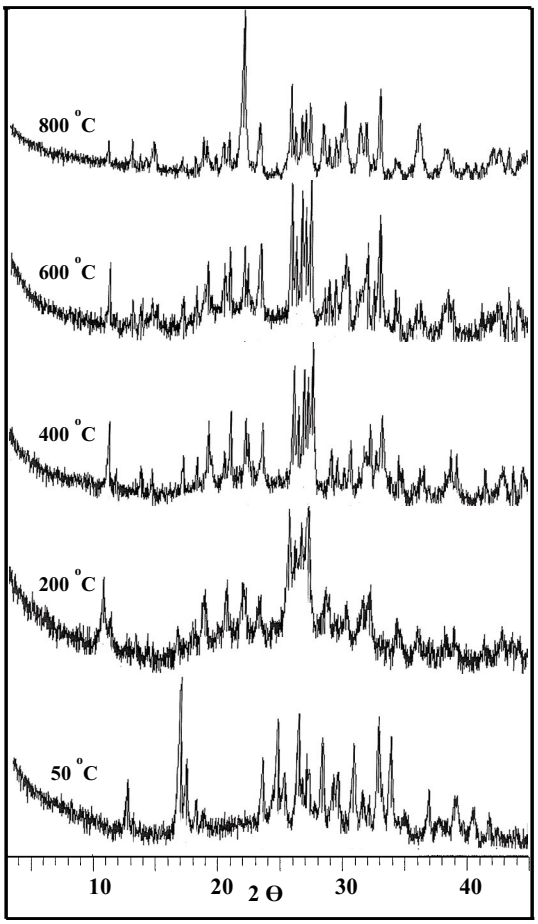

Fig.4. X-ray diffrection pattern of Mn–Si–Mo at different drying temperature.

measurement is water for Mn–Si–Mo substrate. The spectra have been normalized to the sample spectral wavelength of 685 nm characteristic of silica. The absorption peak that appeared around 550 nm could be called a van Hove singularity [43]. The particle distribution was known in the high right corner of Fig. 6 and the average diameter of 1,213 nm was consistent with that from the SEM analysis.

3.2. Distribution studies

Chemical reactions between Mn–Si–Mo and Pb^{2+}, and Fe^{3+} depend on solution pH. Within test pH range between 1 and 6 (Fig. 7), Pb^{2+}, and Fe^{3+} adsorption dropped sharply between pH 1 and 2 and increased further at high pH [33]. Mn–Si–Mo exchanger have pH dependent charges due to protonation and deprotonation of hydroxyl (OH) groups [44,45]. At lower pH, the surface becomes more negative charged and thus, sorbs more Pb^{2+}, and Fe^{3+} oxycations. In general, the lower adsorption of Pb^{2+}, and Fe^{3+} at lower pH might be elucidated by the fact that, at this acidic pH, hydrogen ions may vie with Pb^{2+}, and Fe^{3+} ions for the adsorption sites on adsorbent]. Therefore, at various temperatures (298–328 K), distribution coefficient, were studied and founded that the adsorption efficiency of Mn–Si–Mo was raised with increasing temperature and showed maximum adsorption at 298 K for Pb^{2+}, and Fe^{3+} ions confirmed the endothermic nature of adsorption^{+} [36,46].

3.3. Adsorption capacity

The adsorption capacity of both Pb^{2+} and Fe^{3+} ions on Mn–Si–Mo at different drying temperatures ranging from 50°C to 800°C were investigated. It was reported that the sorption is unfavorable at higher drying temperature. This could be outstanding to (1) occurrence of hydroxyl groups (active sites) onto Mn–Si–Mo surface will evaporate at high drying temperature [33]. (2) The crystallinity will increase with increasing drying temperature and leading to the reformation of the surface structure [47] (Fig. 8), that driving to the diffusion rate of ions during the thermally grew interstitial status of the ion exchange matrix is lower [48,49].

3.4. Adsorption isotherms

Isotherms of Pb^{2+}, and Fe^{3+} (V) adsorption (20–500mg/L) by applying the following equations:

3.4.1. Freundlich form

$$\log q_e = \ln K_F + \frac{1}{n}\log C_e \tag{5}$$

where K_F and n represent adsorption capacity and intensity, respectively. K_F is an important constant used as relative measure for adsorption efficiency, standards of n greater than one show the appreciative nature of adsorption [50,51].

3.4.2. Langmuir form

$$\frac{C_e}{q_e} = \frac{1}{\left(K_L q_m\right)} + \left(\frac{1}{q_m}\right) C_e \tag{6}$$

where q_m is the maximum adsorption capacity (mg/g), K_L is Langmuir constant related to adsorption energy (L/mg). The q_m and K_L can be calculated from the slope and intercept from the plot of C_e/q_e vs. C_e. The results showed that Langmuir, model is not suitable, signifying low affinity by adsorbents since the correlation coefficient is very low (Fig. 9). The adsorbent (Mn–Si–Mo) had good Fe(III) and lead (II) removal efficiency at lower concentrations. At Pb^{2+}, and Fe^{3+} concentration between 20 and 50 mg/L, the Pb^{2+}, and Fe^{3+} removal efficiency was about 90%–100%. Below 50 mg/L Pb(II) and Fe(III), the adsorption is non-linear, while between Pb(II) and Fe(III) 50 and 500 mg/L, the adsorption was fitted with a linear curve. This fact was also proof that different adsorption mechanisms may be concerned, which relied on the initial sorbate concentrations. The isotherm well-fitted with the Freundlich models (Fig. 10, $R^2 > 0.99$) see values of n in (Table 3) [52]. Thermodynamic parameters is the change in free energy of adsorption ($\Delta G°$), enthalpy change ($\Delta H°$), and entropy change ($\Delta S°$)—can be predictable by using the following equation in the temperature range from 25°C to 60°C [53,54]. The values of $\Delta S°$ was calculated from the plot of Gibbs free energy vs temperature for Pb(II) and

Table 2
XRD data of Mn–Si–Mo dried at different drying temperature

Mn–Si–Mo									
50°C		200°C		400°C		600°C		800°C	
2θ	*d*-value (Å)	2θ	*d*-value (Å)	2θ	*d*-value (Å)	2θ	*d*-value (Å)	2θ	*d*-value (Å)
10.62	8.31	11.06	7.99	3.15	27.98	11.06	7.99	10.97	8.05
12.26	7.21	11.69	7.56	11.05	7.99	12.90	6.85	12.90	6.85
12.77	6.92	14.61	6.05	11.59	7.62	13.54	6.53	13.53	6.53
16.48	5.37	17.03	5.2	13.61	6.49	14.87	5.95	14.67	6.03
16.99	5.21	18.24	4.85	14.52	6.09	17.04	5.19	16.93	5.23
17.79	4.98	19.17	4.62	17.03	5.20	18.09	4.89	18.02	4.91
18.38	4.82	20.87	4.25	18.10	4.89	20.32	4.66	18.65	4.75
23.06	3.85	22.13	4.01	19.02	4.66	20.77	4.36	18.93	4.68
24.30	3.65	23.43	3.79	20.28	4.37	21.96	4.27	19.61	4.52
24.81	3.58	25.76	3.45	20.77	4.27	22.22	3.99	20.30	4.36
25.94	3.43	26.23	3.39	21.98	4.04	23.33	3.80	20.74	4.27
26.26	3.39	26.71	3.33	22.22	3.99	25.77	3.45	21.87	4.06
26.56	3.35	27.27	3.26	22.6	3.93	26.16	3.40	23.19	3.83
26.82	3.32	28.68	3.10	23.37	3.80	26.58	3.35	24.59	3.61
27.79	3.20	30.29	2.94	24.65	3.60	26.92	3.30	25.72	3.46
28.32	3.14	31.74	2.81	25.77	3.45	27.30	3.26	26.03	3.41
28.76	3.1	32.22	2.77	26.17	3.40	28.43	3.13	26.55	3.35
29.15	3.06	34.43	2.60	26.60	3.34	28.82	3.09	26.87	3.31
30.35	2.94	36.13	2.48	26.91	3.31	29.31	3.04	27.21	3.27
31.09	2.87	38.28	2.34	27.28	3.26	30.14	2.96	28.31	3.14
31.67	2.82	38.97	2.30	28.85	3.09	30.40	2.93	28.81	3.09
32.33	2.76	41.36	2.18	29.30	3.04	31.95	2.79	29.31	3.04
33.35	2.68	42.77	2.11	29.86	2.98	32.45	2.75	29.7	3.00
34.51	2.59			30.42	2.93	32.87	2.72	30.05	2.97
36.41	2.46			31.02	2.88	32.99	2.71	31.26	2.85
37.25	2.41			31.66	2.82	34.17	2.62	31.81	2.81
38.44	2.33			31.94	2.79	34.55	2.59	32.39	2.76
40.01	2.25			32.88	2.75	35.88	2.50	32.89	2.72
41.24	2.18			33.61	2.66	36.24	2.47	34.12	2.62
41.89	2.15			34.23	2.61	38.44	2.33	35.97	2.49
43.42	2.08			34.51	2.59	38.84	2.31	38.34	2.34
44.59	2.03			35.90	2.49	41.13	2.19	39.78	2.31
				36.23	2.47	42.71	2.11	39.90	2.25
				37.44	2.39	43.33	2.08	40.58	2.22
				38.41	2.34	44.05	2.05	41.09	2.19
				41.16	2.19			41.92	2.15
				42.67	2.11			42.65	2.11
				43.40	2.08			43.32	2.08
				44.08	2.05			44.06	2.05

Fe(III), respectively (Fig. 11). The positive value of $\Delta H°$ reveals the adsorption process is endothermic. On the other hand, sticking probability ($\Delta S°$) of Mn–Si–Mo surface was found to be 0.02 for Pb(II) and 0.1 for Fe(III) which is more than zero, which refers to the process as physisorption. All the values of thermodynamic parameters are reported in Table 4.

3.5. Reaction mechanism

In this research, Mn–Si–Mo exchanger illustrate extraordinary lead and iron adsorption capability with a maximum capacity of 8.5 and 6.5 meq/g, which was mainly due to the presence of more exchanged sites H^+ of Mn–Si–Mo (OH), since H^+ replaced with Pb^{2+}. Even as the Mn–Si–Mo (OH) particles served as the adsorption sites for Pb(II) and Fe(III)

in aqueous solutions and Mn–Si–Mo mainly functioned as ion exchange and the proposed mechanism is ion exchange process. A probable mechanism for the superior selectivity of Pb^{2+} ions contrast to other metal ions (Fe^{3+}) is understood

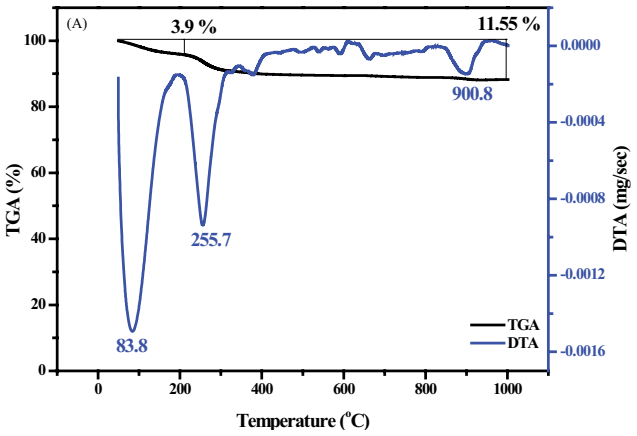

Fig. 5. DTA/TGA thermograms of Mn–Si–Mo.

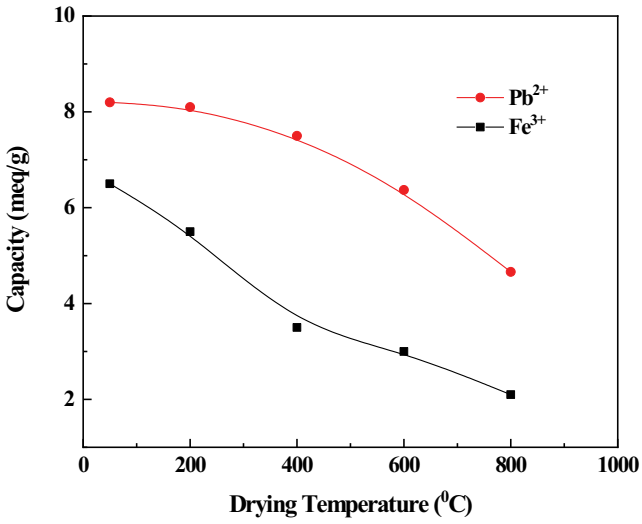

Fig. 8. Adsorption capacity of Pb^{2+}, and Fe^{3+} ions as a function of different drying temperatures.

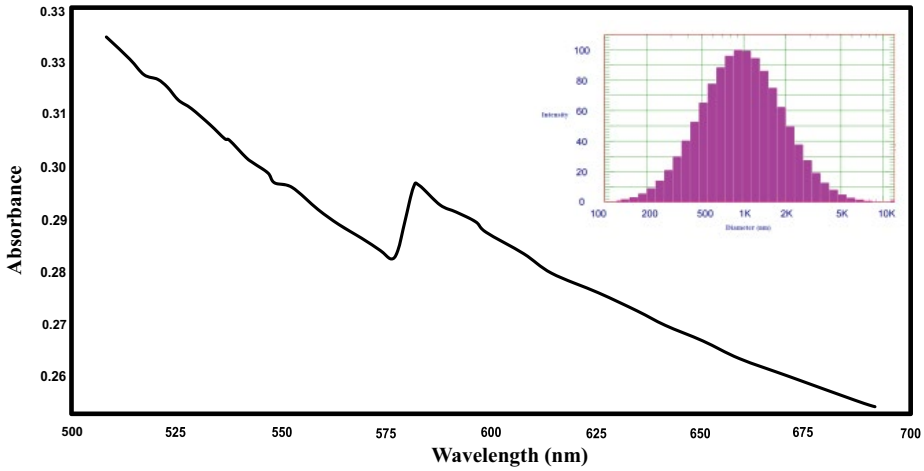

Fig. 6. UV-vis absorption spectrum and size distribution of Mn–Si–Mo suspension.

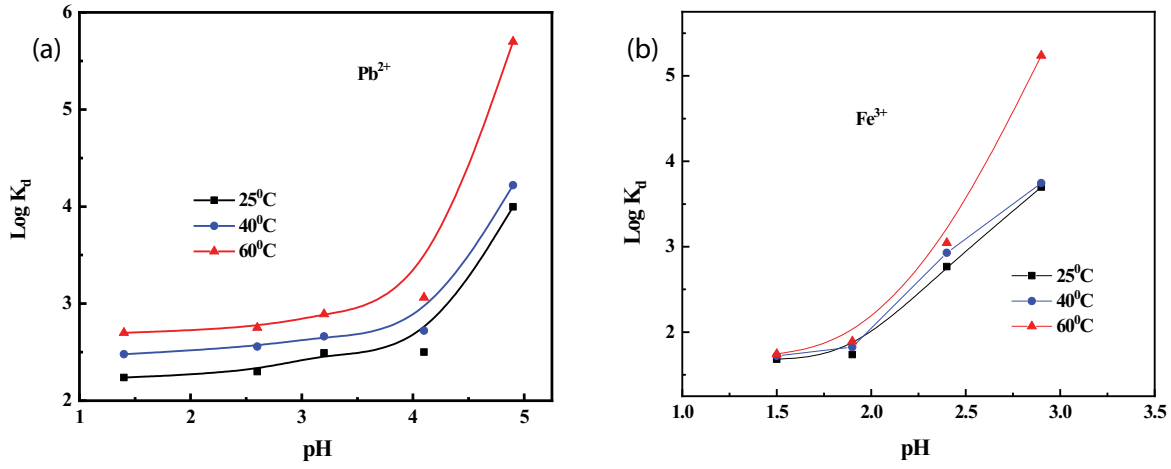

Fig. 7. Plots of pH against log K_d for the exchange of Pb^{2+}, and Fe^{3+} onto Mn–Si–Mo cation exchanger at different reaction temperature.

by taking into account the huge difference stuck between the ionic radii of Pb^{2+} (1.19 Å) and Mn^{2+} (0.7 Å) which directed to Pb^{2+} ions adsorb on Mn–Si–Mo surface. In calculation, the higher Pb^{2+} affinity contrast to Fe^{3+} ions may pointed to that the former ion may be adsorbed on manganese silicomolybdate as unhydrated types. Another means may be implicited in the case of Fe^{3+}, whereas it was indicated that Fe^{3+} ions distorted to steady brown complex with the water molecules (still seen in solution) at low pH region 2 [33]. Transition metals can outline these steady complexes owing to their electronic arrangement (accessibility of d orbital as s and p orbital) [33]. These complex influencing strongly minimizing the positive charge of Fe(III) species. Similar trend was reported for the adsorption of Fe^{3+} on clinoptilolite [55]. Fig. 12 may possibly represent the proposed mechanism during moving of metal ions (Pb^{2+} and Fe^{3+}) from solution to the surface through the pores and lattice channels of Mn–Si–Mo. In fact, oxygen atoms silicate of and molybdate groups are rich in electrons and metal ions (Pb^{2+} and Fe^{3+}) are electropositive. So there was an electrostatic attraction that linked oxygen atoms to metal ions [56].

3.6. Column operations

Since the adsorbate solution deliver through column, the adsorption zone (where most of the adsorption takes place) is released from the column and the concentration of wastewater begins to increase over time. This is called a breakpoint. Breakthrough curve were plotted-gives a ratio of effluent and feed (influent) concentrations (C_e/C_f) and volume (mL) at the operating conditions. In this research, an actual wastewater sample was rounded up from Hesinia city, Egypt. In this study, 850 mL of actual nature water from Hesinia region, East Delta, Egypt acidified with 1 M HNO_3 solution containing a mixture of different concentration of Fe^{3+} and Pb^{2+} ions was push through a glass column packed with 1 g of Mn–Si–Mo at a flow rate 0.6 bed volume/min. Break-through capacities (Q_e) of Pb^{2+} and Fe^{3+} on Mn–Si–Mo are were computed from their corresponding curves shown in Fig. 13. It was established that the break-through capacities are 6.5 and 4.36 meq/g for Pb^{2+}, and Fe^{3+}, respectively.

Table 4
Thermodynamic parameters for the adsorption of Pb^{2+}, and Fe^{3+} onto Mn–Si–Mo at different reaction temperatures

Metal ions	Temperature (K)	$\Delta H°$ (kJ/mol)	$\Delta G°$ (kJ/mol)	$\Delta S°$ (kJ/mol)
	298		–2.53	
Pb^{2+}	313	6.8	–2.71	0.02
	333		–2.91	
	298		–2.38	
Fe^{3+}	313	6.6	–2.55	0.1
	333		–2.74	

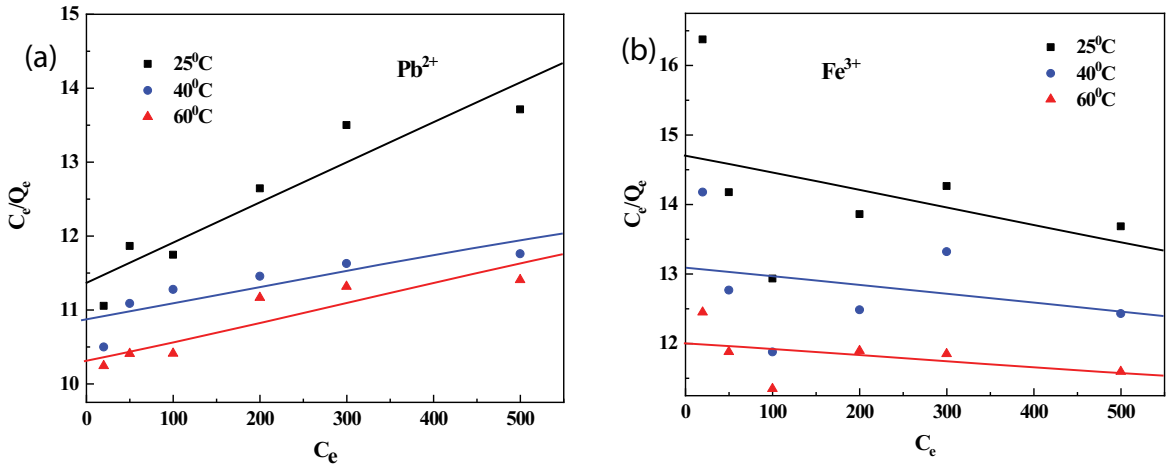

Fig. 9. Langmuir isotherm for adsorption of Pb^{2+} and Fe^{3+} on Mn–Si–Mo.

Table 3
Freundlich isotherm parameters for the sorption of Pb^{2+}, and Fe^{3+} onto Mn–Si–Mo at different reaction temperatures

Metal ions	Temperature (°C)	K_F [(mg/g)/(mg/L)$^{1/n}$]	n	R
Pb^{2+}	25	0.87	1.98	0.99
	40	1.00	1.96	0.99
	60	1.78	1.95	0.99
Fe^{3+}	25	0.41	1.04	0.99
	40	0.64	1.02	0.98
	60	0.96	1.01	0.99

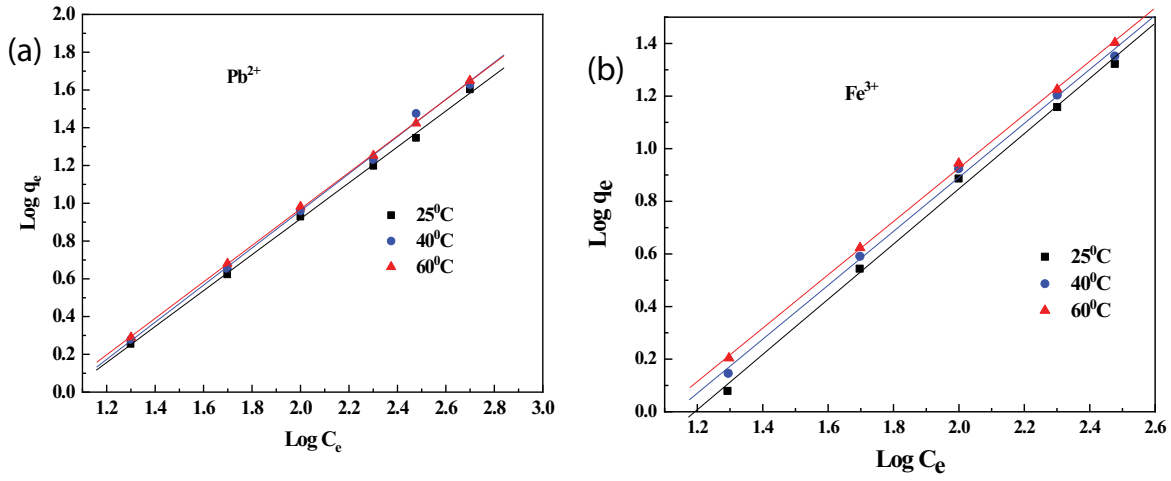

Fig. 10. Freundlich adsorption isotherm for adsorption of Pb^{2+} and Fe^{3+} on Mn–Si–Mo.

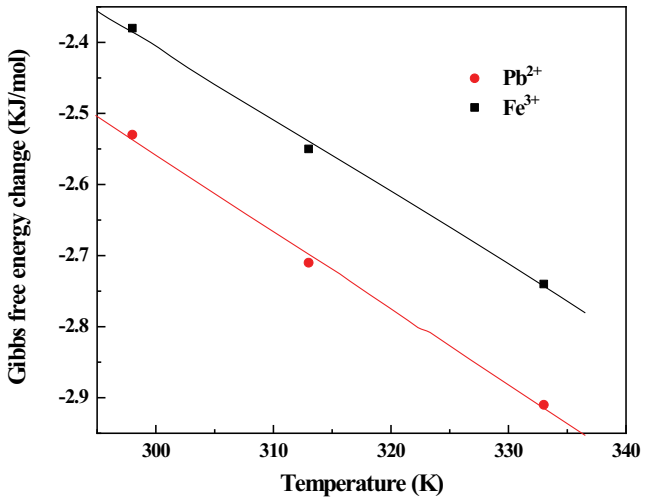

Fig. 11. Plots of Gibbs free energy change at different temperatures

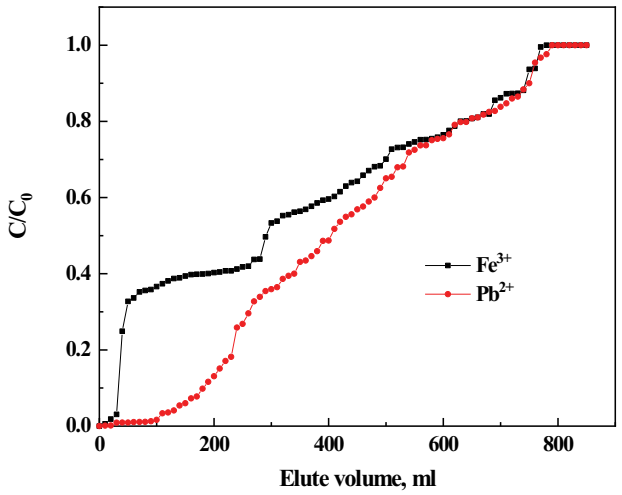

Fig. 13. Breakthrough curves of $Pb^{2}$and Fe^{3+} ions of Mn–Si–Mo at 25°C.

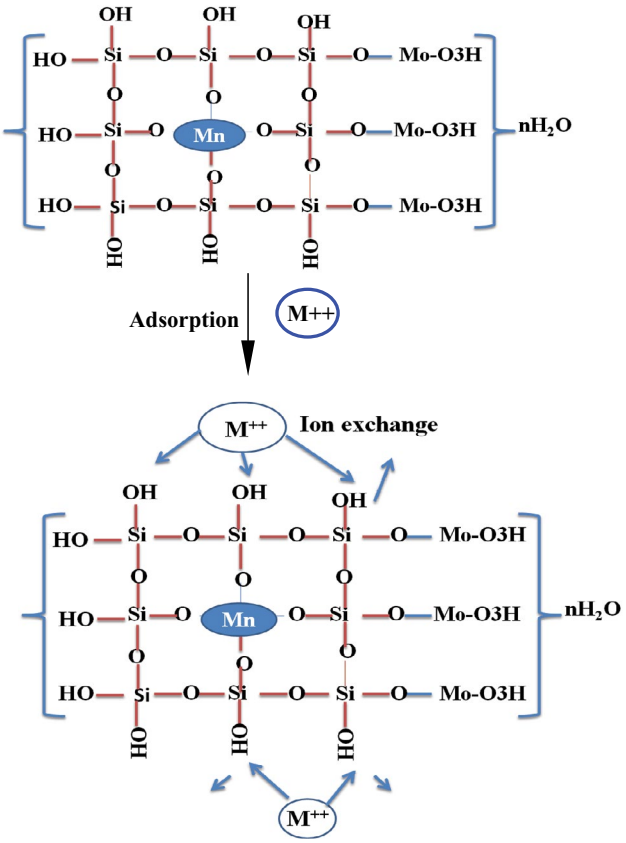

Fig. 12. Adsorption mechanism of metal ion onto Mn–Si–Mo.

4. Conclusion

On the origin of the consequences of the experiments managed, the next conclusions can be confirmed. Mn–Si–Mo has been effectively prepared and applied as a novel and active adsorbent for the elimination of Pb (II), and Fe(III) metal ions from aqueous solution. Mn–Si–Mo was characterized using different tools like SEM, XRD, FTIR, DLS, TGA/

DTA, and UV. The adsorption behavior of heavy metals (lead, and iron toward the prepared material has been studied. The maximum adsorption capacity was established 8.5 and 6.5 meq/g at 25°C for Pb^{2+}, and Fe^{3+} ions respectively. Freundlich isotherm successfully fitted for the adsorption of lead and iron ions which implied that the adsorption process was physi-sorption, the thermodynamic parameters like $\Delta H°$, $\Delta S°$, and $\Delta G°$ were computed, demonstrating that, the adsorption behavior was spontaneous in nature.

References

[1] M.M. Abo-El-Fadl, Possibilities of groundwater pollution in some areas, East of Nile Delta, Egypt, Int. J. Environ., 1 (2013) 1–21.

[2] A. Kortenkamp, M. Casadevall, S.P. Faux, A.A. Jenner, R.O.J. Shayer, N. Woodbrige, P.O. Brien, A role of molecular oxygen in the formation of DNA damage during the reduction of the carcinogen chromium(VI) by glutathione, Arch. Biochem. Biophys., 329 (1996) 199–208.

[3] R. Nazir, M. Khan, M. Masab, H.U. Rehman, N.U. Rauf, S. Shahab, N. Ameer, M. Sajed, M. Ullah, M. Rafeeq, Z. Shaheen, Accumulation of heavy metals (Ni, Cu, Cd, Cr, Pb, Zn, Fe) in the soil, water and plants and analysis of physico-chemical parameters of soil and water collected from Tanda Dam Kohat, J. Pharm. Sci. Res., 7 (2015) 89–97.

[4] J. Kleperis, V. Linkov, M.A. Eddy, Wastewater Engineering, Treatment and Reuse, 4th ed., McGraw-Hill, New York, NY, 2003.

[5] R.F. Aglan, M.M. Hamed, Optimization of environmental friendly process for removal of cadmium from wastewater, Russ. J. Appl. Chem., 87 (2014) 373–382.

[6] I.M. El-Naggar, E.A. Mowafy, E.A. Abdel-Galil, M.F. El-Shahat, Synthesis, characterization and ion-exchange properties of a novel 'Organic-inorganic' hybrid cation exchanger: poly-acrylamide Sn(IV) molybdophosphate, Global J. Phys. Chem., 1 (2010) 91–106.

[7] I.M. El-Naggar, M.Y. Mahmoud, E.A. Abdel-Galil, Inorganic ion exchange materials based on titanate: synthesis, characterization and sorption behavior of zirconium titanate for some hazardous metal ions from aqueous waste solution, Isot. Radiat. Res., 44 (2012) 851–871.

[8] A.M. Adel, A.M. El-Shafei, A.A. Ibrahim, M.T. Al-Shemy, Chitosan/nanocrystalline cellulose biocomposites based on date palm (*Phoenix Dactylifera* L.) sheath fibers, J. Renewable Mater., 7 (2019) 567–582.

[9] I.M. El-Naggar, E.S. Sheneshen, E.A. Abdel-Galil, Retention behavior studies for the removal of some hazardous metal ions from waste solutions using polyaniline silicotitanate as composite cation exchanger, Desal. Water Treat., 56 (2015) 1820–1828.

[10] S. Inoue, H. Maesaki, M. Matsubara, Solvent extraction of copper(II) and lead(II) with N-p-Alkyloxybenzoyl-N-Phenylhydroxylamine, Solvent Extr. Ion Exch., 8 (1990) 257–269.

[11] H. Eccles, Treatment of metal-contaminated wastes: why select a biological process?, Trends Biotechnol., 17 (1999) 462–465.

[12] W.C. Leung, M.F. Wong, H. Chua, W. Lo, C.K. Leung, Removal and recovery of heavy metals by bacteria isolated from activated sludge treating industrial effluents and municipal waste-water, Water Sci. Technol., 41 (2000) 233–240.

[13] N.E. Dávila-Guzmán, F.J. Cerino-Córdova, E. Soto-Regalado, J.R. Rangel-Mendez, P.E. Díaz-Flores, M.T. Garza-Gonzalez, J.A. Loredo-Medrano, Copper biosorption by spent coffee ground: equilibrium, kinetics, and mechanism, Clean Soil Air Water, 41 (2013) 557–564.

[14] X. Tang, Z. Li, Y. Chen, Adsorption behavior of Zn(II) on calcinated Chinese loess, J. Hazard. Mater., 16 (2009) 824–834.

[15] M. Betancur, P.R. Bonelli, J.A. Velásquez, A.L. Cukierman, Potentiality of lignin from the Kraf pulping process for removal of trace nickel from wastewater: effect of demineralisation, Bioresour. Technol., 100 (2009) 1130–1137.

[16] K. Rouibah, A. Meniai, M.T. Rouibah, L. Deffous, M.B. Lehocine, Elimination of chromium(VI) and cadmium(II) from aqueous solutions by adsorption onto olive stones, Open Chem. Eng. J., 3 (2009) 41–48.

[17] M. Sprynskyy, T. Kowalkowski, H. Tutu, E.M. Cukrowska, B. Buszewski, Adsorption performance of talc for uranium removal from aqueous solution, Chem. Eng. J., 171 (2011) 1185–1193.

[18] A. León-Torres, E.M. Cuerda-Correa, C. Fernández-González, M.F. Alexandre Franco, V. Gomez-Serrano, On the use of a natural peat for the removal of Cr(VI) from aqueous solutions, J. Colloid Interface Sci., 386 (2012) 325–332.

[19] M. Sprynskyy, I. Kovalchuk, B. Buszewski, The separation of uranium ions by natural and modified diatomite from aqueous solution, J. Hazard. Mater., 181 (2010) 700–707.

[20] M.A. Ashraf, M.A. Rehman, Y. Alias, I. Yusoff, Removal of Cd(II) onto *Raphanus sativus* peels biomass: equilibrium, kinetics, and thermodynamics, Desal. Water Treat., 51 (2013) 4402–4412.

[21] J. Zhu, V. Cozzolino, M. Pinga, Q. Huang, C. Giandonato, A. Violante, Sorption of Cu, Pb and Cr on Na-montmorillonite: competition and effect of major elements, Chemosphere, 84 (2011) 484–489.

[22] M. Sprynskyy, B. Buszewski, A.P. Terzyk, J. Namieśnik, Study of the selection mechanism of heavy metal (Pb^{2+}, Cu^{2+}, Ni^{2+}, and Cd^{2+}) adsorption on clinoptilolite, J. Colloid Interface Sci., 304 (2006) 21–28.

[23] H. Wang, F. Yin, B. Chen, G. Li, Synthesis of an ε-MnO_2/metal–organic framework composite and its electrocatalysis towards oxygen reduction reaction in an alkaline electrolyte, J. Mater. Chem. A, 3 (2015) 16168–16176.

[24] D. Chen, W. Shen, S. Wu, C. Chen, X. Luo, L. Guo, Ion exchange induced removal of Pb(II) by MOF-derived magnetic inorganic sorbents, Nanoscale, 8 (2016) 7172–7179.

[25] R. Ricco, K. Konstas, M.J. Styles, J.J. Richardson, R. Babarao, K. Suzuki, P. Scopece, P. Falcaro, Lead(II) uptake by aluminium based magnetic framework composites (MFCs) in water, J. Mater. Chem. A, 3 (2015) 19822–19831.

[26] P.A. Kobielska, A.J. Howarth, O.K. Farha, S. Nayak, Metal–organic frameworks for heavy metal removal from water, Coord. Chem. Rev., 358 (2018) 92–107.

[27] X. Li, C. Bian, X. Meng, F.S. Xiao, Design and synthesis of an efficient nanoporous adsorbent for Hg^{2+} and Pb^{2+} ions in water, J. Mater. Chem. A, 4 (2016) 5999–6005.

[28] Q.F. Liu, N. Jiang, C.L. Che, F. Chu, Adsorption properties of POMS/CTS composite materials on Pb^{2+} in water analyzed by T tese and nonparametric test, Sci. Bull., 81 (2019) 1–10.

[29] A. Abbasi, T. Moradpour, K. Van Hecke, A new 3D cobalt(II) metal–organic framework nanostructure for heavy metal adsorption, Inorg. Chim. Acta, 430 (2015) 261–267.

[30] A.M. Puziy, O.I. Poddubnaya, A. Martınez-Alonso, F. Suárez-Garcıa, J.M.D. Tascón, Synthetic carbons activated with phosphoric acid: I. Surface chemistry and ion binding properties, Carbon, 40 (2002) 1493–1505.

[31] F. Gai, T. Zhou, G. Chu, Y. Li, Y. Liu, Q. Huo, F. Akhtar, Mixed anionic surfactant-templated mesoporous silica nanoparticles for fluorescence detection of Fe^{3+}, Dalton Trans., 45 (2016) 508–514.

[32] E.R. Soliman, Y.H. Kotp, E.R. Souaya, K.A. Guindy, R.G. Ibrahim, Development the sorption behavior of nanocomposite Mg/Al LDH by chelating with different monomers, Composites Part B, 175 (2019) 107131.

[33] I.M. Ali, Y.H. Kotp, I.M. El-Naggar, Thermal stability, structural modifications and ion exchange properties of magnesium silicate, Desalination, 259 (2010) 228–234.

[34] A. Adel, A. El-Shafei, A. Ibrahim, M. Al-Shemy, Extraction of oxidized nanocellulose from date palm (*Phoenix dactylifera* L.) sheath fibers: influence of CI and CII polymorphs on the properties of chitosan/bionanocomposite films, Ind. Crops Prod., 124 (2018) 155–165.

[35] Y.H. Kotp, Controlled synthesis and sorption properties of magnesium silicate nanoflower prepared by a surfactant-mediated method, Sep. Sci. Technol., 52 (2017) 657–670.

[36] Y.H. Kotp, M.E. Ali, S.A. Mohallal, M.M. Aboelfadl, Synthesis of a novel inorganic cation exchanger based on molybdate: applications for removal of Pb^{2+}, Fe^{3+} and Mn^{2+} ions from polluted water, Sep. Sci. Technol., 54 (2019) 620–633.
[37] Y.H. Kotp, Removal of organic pollutants using polysulfone ultrafiltration membrane containing polystyrene silicomolybdate nanoparticles: case study: Borg El Arab area, J. Water Process Eng., 30 (2019) 100553.
[38] I.M. Ali, M.Y. Nassar, Y.H. Kotp, M. Khalil, Cylindrical-design, dehydration, and sorption properties of easily synthesized magnesium phosphosilicate nanopowder, Part. Sci. Technol., 37 (2019) 207–219.
[39] A.M. El-Shafei, A.M. Adel, A.A. Ibrahim, M.T. Al-Shemy, Dual functional jute fabric biocomposite with chitosan and phosphorylated nano-cellulose (antimicrobial and thermal stability), Int. J. Biol. Macromol., 124 (2019) 733–741.
[40] Y.H. Kotp, Y.A. Shebl, M.S. El-Deab, B.E. El-Anadouli, H.A. Shawky, Performance enhancement of PA-TFC RO membrane by using magnesium silicate nanoparticles, J. Inorg. Organomet. Polym., 27 (2017) 201–214.
[41] K.S. Rao, K. El-Hami, T. Kodaki, K. Matsushige, K. Makino, A novel method for synthesis of silica nanoparticles, J. Colloid Interface Sci., 289 (2005) 125–131.
[42] V. Tharanitharan, R. Kalaivani, Adsorption of heavy metal ions from water and wastewater using modified acrylic ester polymeric resin, Chem. Sci. Rev. Lett., 2 (2014) 393–401.
[43] A.M. Ziyath, P. Mahbub, A. Goonetilleke, M.O. Adebajo, S. Kokot, A. Oloyede, Influence of physical and chemical parameters on the treatment of heavy metals in polluted stormwater using zeolite—a review, J. Water Resour. Prot., 3 (2011) 758–767.
[44] E.A. Abdelrahman, R.M. Hegazey, Y.H. Kotp, A. Alharbi, Facile synthesis of Fe_2O_3 nanoparticles from Egyptian insecticide cans for efficient photocatalytic degradation of methylene blue and crystal violet dyes. Spectrochim. Acta, Part A, 222 (2019) 117195.
[45] L. Chen, B.Y. He, S. He, T.J. Wang, C.L. Su, Y. Jin, Fe–Ti oxide nano-adsorbent synthesized by co-precipitation for fluoride removal from drinking water and its adsorption mechanism, Powder Technol., 227 (2012) 3–8.
[46] F. Gode, E. Pehlivan, Adsorption of Cr(III) ions by Turkish brown coals, Fuel Process. Technol., 86 (2005) 875–884.
[47] R. Naseem, S.S. Tahir, Removal of Pb(II) from aqueous/acidic solutions by using bentonite as an adsorbent, Water Res., 35 (2001) 3982–3986.
[48] H.M. Aly, M.E. Moustafa, E.A. Abdelrahman, Influence of aluminum source on the synthesis of nanosized ZSM-5 zeolite, Der Chem. Sin., 4 (2013) 68–72.
[49] E.A. Abdelrahman, R.M. Hegazey, Exploitation of Egyptian insecticide cans in the fabrication of Si/Fe nanostructures and their chitosan polymer composites for the removal of Ni(II), Cu(II), and Zn(II) ions from aqueous solutions, Composites Part B, 166 (2019) 382–400.
[50] P.R. Rout, P. Bhunia, R.R. Dash, Modeling isotherms, kinetics and understanding the mechanism of phosphate adsorption onto a solid waste: ground burnt patties, J. Environ. Chem. Eng., 2 (2014) 1331–1342.
[51] E.A. Abdelrahman, R.M. Hegazey, Facile synthesis of HgO nanoparticles using hydrothermal method for efficient photocatalytic degradation of crystal violet dye under UV and sunlight irradiation, J. Inorg. Organomet. Polym. Mater., 29 (2019) 346–358.
[52] K. Gong, Y. Liu, Manganese-phosphomolybdate molecular catalysts for the electron transfer reaction of ferricyanide to ferrocyanide, RSC Adv., 5 (2015) 47004–47009.
[53] M.V. Sivaiah, K.A. Venkatesan, R.M. Krishna, P. Sasidhar, G.S. Murthy, Characterization of uranium antimonite ion exchanger, Colloids Surf., A, 295 (2007) 1–6.
[54] G. Sharma, M. Naushad, A.H. Al-Muhtaseb, A. Kumar, M. Rizwan, K. Susheel, K. Shweta, M. Bala, A. Sharma, Fabrication and characterization of chitosan-crosslinked-poly (alginic acid) nanohydrogel for adsorptive removal of Cr(VI) metal ion from aqueous medium, Int. J. Biol. Macromol., 95 (2017) 484–493.
[55] Y. Masue, R.H. Loeppert, T.A. Kramer, Arsenate and arsenite adsorption and desorption behavior on coprecipitated aluminum: iron hydroxides, Environ. Sci. Technol., 41 (2007) 837–842.
[56] S. Al-Saadon, Inhibition of Copper-Mild Steel Galvanic Corrosion, The University of Manchester, United Kingdom, 2005.